Original paper

Electrodeposited hydroxyapatite coating on titanium after ultrashort-pulsed laser processing for a novel surface of endosseous implants

Magdalena Łukaszewska-Kuska[1,A–F], Piotr Krawczyk[2,A–C,E,F], Tomasz Buchwald[3,B,C,E,F], Agnieszka Martyła[4,B,C,E,F], Viktor Zinchenko[5,B,C,E,F], Radomir Majchrowski[6,B,C,E,F], Robert Edward Przekop[4,B,E,F], Barbara Dorocka-Bobkowska[1,A,E,F]

[1] Department of Prosthetic Dentistry and Gerodontology, Poznan University of Medical Sciences, Poland
[2] Institute of Chemistry and Technical Electrochemistry, Poznan University of Technology, Poland
[3] Institute of Material Research and Quantum Engineering, Poznan University of Technology, Poland
[4] Centre for Advanced Technology, Adam Mickiewicz University, Poznań, Poland
[5] Department of Chemistry of Functional Inorganic Materials, A.V. Bogatsky Physico-Chemical Institute of the National Academy of Sciences of Ukraine, Odessa, Ukraine
[6] Division of Metrology and Measurement Systems, Institute of Mechanical Technology, Poznan University of Technology, Poland

A – research concept and design; B – collection and/or assembly of data; C – data analysis and interpretation;
D – writing the article; E – critical revision of the article; F – final approval of the article

Dental and Medical Problems, ISSN 1644-387X (print), ISSN 2300-9020 (online) *Dent Med Probl*. 2024;61(6):909–918

Address for correspondence
Magdalena Łukaszewska-Kuska
E-mail: mluk@ump.edu.pl

Funding sources
The research was funded by the National Science Centre (NCN), Poland (grant No. 2021/05/X/ST5/00773). Raman spectroscopy analysis was carried out with financial support from the Polish Ministry of Science and Higher Education (No. 0511/SBAD/2451).

Conflict of interest
None declared

Acknowledgements
The authors would like to thank Iaroslav Gnilitskyi, Vasyl Kurylo and Maksym Kyrychok from NoviNano Lab LLC, Lviv, Ukraine, for laser modification and static contact angle studies.

Received on October 27, 2023
Reviewed on November 12, 2023
Accepted on November 21, 2023

Published online on December 20, 2024

Cite as
Łukaszewska-Kuska M, Krawczyk P, Buchwald T, et al. Electrodeposited hydroxyapatite coating on titanium after ultrashort-pulsed laser processing for a novel surface of endosseous implants. *Dent Med Probl.* 2024;61(6):909–918. doi:10.17219/dmp/175612

DOI
10.17219/dmp/175612

Abstract

Background. Ceramic endosseous implant coatings have gained esteem due to their favorable osteoinductive and osteoconductive properties. However, such a layer may be prone to failure under in vivo conditions, which necessitates its modification.

Objectives. The aim of the present study was to modify an electrodeposited hydroxyapatite (HA) coating on titanium (Ti) with ultrashort-pulsed lasers for the incorporation of the ceramic into the sample surface and the texturing of the metal surface. The obtained surface was planned for application on the endosseous implant surface to enhance osseointegration. To our knowledge, such laser modification of a HA coating has not been performed previously.

Material and methods. Four different HA coatings were created (A–D). Each coating was conditioned with 4 different laser irradiations (1-4 to 4-4), carried out using different power, velocity and frequency settings. The surface features of the laser-irradiated coatings were analyzed.

Results. The laser modifications of the HA coatings resulted in 2 kinds of surfaces. Laser-induced periodic surface structure (LIPSS) texturing could be observed on quadrants 1-4 to 3-4, with parallel grooves and HA crystals melted and sintered into spherical structures. The 4-4 laser surface conditioning did not altered the needle-like morphology of the HA coating. The LIPSS–fusion modification decreased the water contact angle of the samples.

Conclusions. The ultrashort-pulsed laser modification of the HA coating for regimes 1-4 to 3-4 resulted in the LIPSS texturing of the Ti surface with HA sinterization. Further biological analyses are necessary to evaluate the cell and tissue response to such laser-modified HA coating on Ti.

Keywords: titanium, hydroxyapatite, laser processing, periodic surface structure texturing

Introduction

Osseointegration, defined as a direct structural and functional connection between ordered living bone and the surface of a load-carrying implant, is a key factor of clinical success in dental implant rehabilitation.[1,2] The goal of modern implantology is rapid and strong osseointegration. There are many factors affecting osseointegration, such as implant factors, host factors, the surgical technique, the healing time, and the loading conditions.[3] Among implant factors, implant composition, biocompatibility, macroscopic and microscopic surface topography and treatment, osteogenic biological coatings, surface energy, and wettability can influence the osseointegration process.[3] Continuous research is focused on developing an implant with features favoring osseointegration. There are numerous procedures to modify the implant surface. Surface topography can be modified by blasting or etching.[4,5] A biological coating can be obtained by adding compounds affecting osteoblasts, such as hydroxyapatite (HA).[6,7] Wettability can be improved by the immersion of the modified titanium (Ti) implant in an isotonic solution at low pH or by photo-functionalization.[2,8]

One of the more recent techniques of surface modification is laser treatment. Precise, organized, nano- or micrometer surface structures,[9,10] can be manufactured using this technique, with a reduced risk of surface contamination.[11] Among different kinds of laser surface treatment, ultrashort-pulsed lasers have recently been investigated as a potential structuring tool for biomedical implants.[12,13] The technique focuses energy in time and space, resulting in laser-induced periodic surface structure (LIPSS) texturing, with minimal thermal damage. The LIPSS are self-organized formations observed on the surfaces treated with polarized laser radiation.[10]

Hydroxyapatite, $Ca_{10}(PO_4)_6(OH)_2$, is a mineral from the family of apatites.[14,15] It is a natural component of bones and tooth tissue. Hydroxyapatite in the form of crystals provides the structural stability and hardness of the bone. It is also involved in the bone regeneration process, since it exhibits osteoinductive and osteoconductive properties. Synthetic HA, on the other hand, is currently used for bone repair, as well as for bone regeneration. In implantology, HA coatings on the implant surface have been used for many years as bioactive coatings.[16,17] Such a ceramic coating improves osseointegration and provides long-term in vivo functionality.[16,17] Those features are related to the great capacity of HA for adsorbing proteins, improving osteoblast proliferation, enhancing bone formation, reducing bone loss, and augmenting osteogenic activity through the direct release of calcium (Ca) and phosphate ions.[7,17,18] Hydroxyapatite used as a coating for endosseous implants has been reported to be an effective material for the bone–implant interface because of its similarity to the mineral phase of natural bone tissue.[7] Hydroxyapatite coatings can be applied on the implant surface with different techniques, such as plasma spraying, biomimetic deposition, the sol–gel technique, or electrophoretic deposition.[7,14,17] Some techniques, i.e., plasma spraying, utilize high temperatures, generating a large amount of amorphous HA and providing a microcracked thick coating.[7,14] Such a layer is prone to failure under in vivo conditions because of its high bio-dissolution rate, disintegration with the formation of debris particles, and the risk of delamination caused by low bond strength with Ti.[14,17] Conversely, the electrodeposition of HA is conducted at relatively low temperatures, eliminating the risk of the synthesis of amorphous HA.[19] The dissolution and bond strength degradation of the electrodeposited coatings are reported to be much lower than those of the plasma-sprayed coatings.[19,20] Also, a coating thickness of less than 1 μm increases delamination resistance.[19,21] The electrodeposition process can also result in good conformability to the shape of the component and in coating homogeneity.[19] However, the elevated temperature during electrodeposition results in decreased coating adhesion to the substrate as compared to the processes conducted at room temperature.[19,22] To incorporate HA into the Ti surface and reduce the risk of delamination, laser conditioning is applied. The obtained LIPSS are also meant to enhance cell differentiation, improving the osseointegration of such modified endosseous implants.[23,24]

In this article, we present a thin HA coating on Ti, obtained by electrophoretic deposition processed with laser irradiation, using different laser parameters, for the incorporation of the ceramic into the sample surface and the texturing of the metal surface. The influence of laser irradiation on the ceramic coating was analyzed, and the modification with the most promising osteoconductive properties was determined. To our knowledge, such laser modification of HA coatings has not been performed previously.

Material and methods

Sample preparation

The samples were prepared from Ti grade 4 ASTM B348 EN10204/3.1. Disks with a diameter of 14 mm and a thickness of 2 mm were milled from Ti rods. The sample surface was sandblasted using alumina (Al_2O_3) with a particle size of 53–75 μm at a pressure of 4 atm.

Electrochemical deposition of hydroxyapatite

The HA coating was electrodeposited on a working electrode – commercially pure Ti disks with a diameter of 14 mm and a thickness of 2 mm, fused with the Ti rod. As a counter electrode, a 10 cm × 10 cm platinum (Pt) mesh was used. The electrolyte was composed of 4.16×10^{-4} M $CaCl_2$, 2.5×10^{-4} M NaH_2PO_4 and 0.2 M NaCl in

distilled water, with pH adjusted to 6.3. An Autolab potentiostat-galvanostat (PGSTAT302N; Metrohm Autolab, Utrecht, the Netherlands) with a 2-electrode system in a galvanostatic mode was used. The process was carried out in a 100 mL 3-neck flask, used as an electrochemical reactor, immersed in an oil bath at 105°C. Electrodeposition was conducted for 60 min with a current of 5 mA, 120 min with a current of 30 mA, 120 min with a current of 10 mA, and 60 min with a current of 30 mA for samples A–D, respectively.

The electrodeposition of HA on a Ti surface occurs according to the following chemical reaction: $10Ca^{2+} + 6PO_4^{3-} + 2OH^- \rightarrow Ca_{10}(PO_4)_6(OH)_2$. Such a reaction is triggered by the increased pH on the cathode surface, caused by the formation of hydroxide ions from the reduction of water $2H_20 + 2e \rightarrow 2OH^- + H_2$. The pH alteration generates a critical supersaturation status at the interface of the electrode and the electrolyte for the precipitation of HA, and triggers the nucleation and growth of the HA coating.[25]

Laser treatment

The laser experimental setup shown in Fig. 1 was used for the sintering of HA particles on a Ti substrate. A laser system (Pharos P-20; Light Conversion, Vilnius, Lithuania) providing femtosecond pulses (τ = 213 fs) at a central wavelength of 1,030 nm with a spectral width of 15 nm, $M^2 \simeq 1.1$, was used. Upon irradiation, the Ti samples were fixed on the Ti substrate in an air atmosphere, and the laser beam was focused on the Ti surface with a spot diameter of 10.4 µm (at level 1/e2). A scanning mode with various overlaps was used for irradiation.

The surface of each Ti disk was divided into 4 quadrants. Each quadrant was numbered from 1-4 to 4-4, and was modified according to the parameters presented in Table 1.

Surface analysis

A Hitachi S-3400N scanning electron microscope (SEM) (Hitachi High-Technologies Corporation, Tokyo, Japan) was used to obtain micrographs of the investigated samples. Two magnifications, ×1,000 and ×5,000, were used. Contact profilometry was performed to analyze surface roughness. A T8000 profilometer (Hommel-Etamic, Herrenberg, Germany) with the EVOVIS software was used. Each quadrant was analyzed on the 3 profiles. An experimental sector of 8.0 mm was selected in accordance with PN-EN ISO 4287. A total number of 48 analyses were performed. Parameters Ra, Rt and RSm were measured. The results were expressed as mean ± standard deviation (*M* ±*SD*).

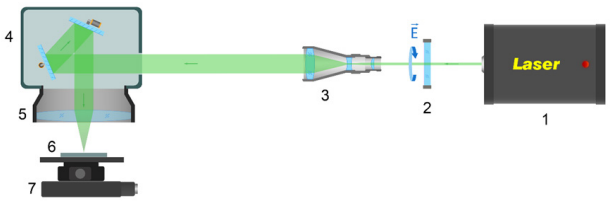

Fig. 1. Laser experimental setup

1 – laser; 2 – polarizer; 3 – telescope; 4 – galvanoscanner; 5 – lens; 6 – sample; 7 – coordinate table.

Table 1. Parameters for the laser modifications of the hydroxyapatite (HA)-coated titanium (Ti) samples

Quadrant	Modification	P [W]	V [m/s]	RR [kHz]	Steps per µm
1-4	LIPSS	0.33	1.000	500	5
	fusion	0.50	0.050	500	5
2-4	sintering	1.00	0.075	1,000	5
3-4	sintering	1.00	0.100	1,000	5
4-4	sintering	0.80	0.100	1,000	5

P – power; V – velocity; RR – frequency; LIPSS – laser-induced periodic surface structures.

Surface chemical composition

The chemical composition of the surface was determined using the energy-dispersive spectroscopy (EDS) analysis, the X-ray diffraction (XRD) analysis and the Raman spectroscopy analysis. The semi-quantitative chemical composition of the samples was determined using EDS (model No. 4481B-1UES-SN with the NSS Spectral Imaging System software; Thermo Fisher Scientific, Waltham, USA). The Raman spectroscopy analysis was conducted using the inVia™ Raman system (Renishaw, Wotton-under-Edge, UK). Raman spectra were collected in the spectral range of 200–4,000 cm^{-1}, using a 785 nm laser and a 1,200 l/mm diffraction grating. The XRD analysis was performed using an XRD diffractometer (D8 Advance; Bruker, Billerica, USA) with copper (Cu) lamp radiation. X-ray spectra were recorded in the angular range of 20–80° 2Θ, with a step size of 0.02° and a normalized count time of 2 s/step. The XRD analysis was conducted for each section of the disk. Lead (Pb) foil covered the 3 quadrants not being analyzed. The diffraction patterns in the angle range of HA reflexes were also performed. The identification of HA was based on the literature and the International Centre for Diffraction Data (ICDD 01-086-0740 data).[26–28]

Static contact angle studies

The contact angle of the sample surfaces was measured using a Theta Flex optical tensiometer (Biolin Scientific, Västra Frölunda, Göteborg, Sweden) at room temperature (22°C). The water contact angle of the 4 quadrants of each sample was evaluated by static contact angle measurements, utilizing the sessile drop method. A 1-microliter droplet of distilled water was placed on the dry

surface of each quadrant of the studied sample, and the image of the drop was recorded for 10 s. An average value of the contact angle was calculated based on at least 5 measurements. The static contact angle was then defined by fitting the Young–Laplace equation to the droplet. The results were expressed as $M \pm SD$.

Results

Surface analysis

Morphology and topography studies

The SEM images of the HA coating after electrodeposition and laser modification are presented in Fig. 2. The HA coating on sample A-4-4 presented a layer of spherical crystals with a diameter of less than 5 µm. Hydroxyapatite crystals did not completely cover the Ti surface. On sample B-4-4, the HA coating was composed of a continuous layer of needle-like crystals with a diameter of about 5 µm and a length of up to 20 µm. The HA coating was dense, with tightly packed crystals. The surface of sample C-4-4 was covered in short, needle-like crystals with a diameter of about 2 µm and a length of up to 5 µm. The crystals were not covering the Ti surface continuously. Sample D-4-4 was covered by a layer of short, needle-like crystals with a diameter of 1 µm and a length of 2 µm. The sample surface was not completely covered with crystals, and the packing of the crystals was not as dense as in the case of the B samples. On top of the layer of short crystals, foci of long, needle-like crystals with a diameter of 5 µm and length of up to 60 µm were present. Laser modifications from 1-4 up to 3-4 eliminated the needle-like shape of the crystals. Spherical structures were present after such modifications. Also, the Ti surface was modified. After laser modifications 1-4 to 3-4, the Ti surface exhibited parallel grooves with a width of about 2 µm. The depth of the grooves increased from 3-4 up to 1-4 modifications. Limited flat areas of the sample surfaces were not covered by grooves and presented spherical structures of about 1 µm in diameter.

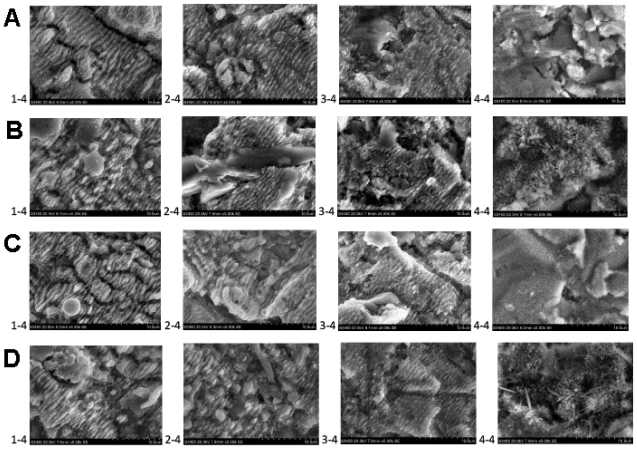

Fig. 2. Scanning electron microscopy (SEM) images of the electrodeposited hydroxyapatite (HA) after laser modifications, quadrants 1-4 to 4-4 magnification ×5,000.

Contact profilometry

The roughness of the analyzed surfaces expressed as Ra and Rt is presented in Table 2. The Ra values, which are the arithmetic means of the absolute values of the roughness profile ordinates, ranged from 1.32 µm for C-4-4 up to 1.85 µm for A-1-4. For samples B and C, the 2-4 type of laser conditioning resulted in the highest Ra parameters, whereas for samples A and D, the highest Ra parameters were found in conditions 1-4 and 3-4, respectively. The parameter Rt, defined as the total height of the profile, is the vertical distance between the maximum profile peak height and the maximum profile valley depth along the evaluation length. The Rt values for the analyzed samples ranged from 10.65 µm for sample C-4-4 up to 17.12 µm for sample C-2-4. The highest Rt values were noted for the 1-4 laser modification for samples A and B, and for the 2-4 and 4-4 modifications for samples C and D, respectively.

Surface chemical composition

Energy-dispersive spectroscopy (EDS) analysis

The EDS analysis revealed the peaks mainly from Ti, oxygen (O), Ca, phosphorus (P), and aluminum (Al) (Table 3).

Table 2. Surfaces roughness parameters (Ra and Rt) for 4 different laser modifications of the analyzed samples

Sample and quadrant	Ra [µm]	Rt [µm]
A-4-4	1.67 ±0.04	14.73 ±0.80
A-3-4	1.56 ±0.07	14.82 ±0.82
A-2-4	1.66 ±0.07	14.25 ±1.71
A-1-4	1.85 ±0.12	15.09 ±3.31
B-4-4	1.70 ±0.18	15.17 ±0.98
B-3-4	1.68 ±0.05	13.68 ±1.23
B-2-4	1.79 ±0.12	14.94 ±2.30
B-1-4	1.72 ±0.04	15.74 ±1.10
C-4-4	1.32 ±0.13	10.65 ±1.45
C-3-4	1.50 ±0.04	15.19 ±0.24
C-2-4	1.73 ±0.05	17.12 ±2.70
C-1-4	1.50 ±0.07	14.06 ±1.36
D-4-4	1.60 ±0.11	15.81 ±2.71
D-3-4	1.74 ±0.06	14.66 ±1.60
D-2-4	1.60 ±0.10	13.09 ±0.10
D-1-4	1.70 ±0.06	14.89 ±2.08

Data presented as mean ± standard deviation ($M \pm SD$).

Table 3. Energy-dispersive spectroscopy (EDS) analysis of the hydroxyapatite (HA) coating with laser sintering, concerning the oxygen (O), calcium (Ca), phosphorus (P), and carbon (C) concentrations, expressed as weight percent (wt%)

Sample and quadrant	Ti	O	Ca	P	C
A-4-4	54.76	32.45	0.47	0.31	1.08
A-3-4	61.19	22.67	0.03	0.04	0.83
A-2-4	71.21	27.93	0.01	0.04	0.77
A-1-4	69.63	18.99	0.02	0.05	1.27
B-4-4	39.38	36.39	9.01	5.04	1.91
B-3-4	57.33	32.32	0.61	0.40	0.63
B-2-4	73.78	18.87	1.71	1.06	1.12
B-1-4	77.16	19.79	0.55	0.36	2.14
C-4-4	52.75	33.77	1.84	1.07	1.51
C-3-4	61.47	30.78	0.24	0.16	0.50
C-2-4	64.69	24.50	0.07	0.09	0.72
C-1-4	81.01	13.41	0.07	0.05	0.48
D-4-4	45.95	34.67	2.72	1.86	1.47
D-3-4	63.00	23.23	0.05	0.10	1.06
D-2-4	63.57	21.07	0.04	0.09	1.43
D-1-4	73.92	17.05	0.13	0.10	0.98

The concentrations of Ca and P were the highest on the 4-4 quadrants. Among those quadrants, the Ca and P concentrations were the highest for sample B and the lowest for sample A. Laser processing 1-4 up to 3-4 resulted in a decrease in the Ca and P concentrations. In most cases, a decrease in the Ca and P concentrations could be observed with the change of laser modification from 3-4 to 1-4.

The O concentrations were the highest on the 4-4 quadrants. The level of oxygen decreased from quadrants 3-4 to 1-4.

For samples A and B, the highest C concentrations were observed for quadrants 1-4, and the lowest for quadrants 2-4 and 3-4, respectively. For samples C and D, the highest C concentrations were noted for quadrants 4-4, and the lowest for quadrants 1-4. For laser-sintered quadrants, the highest C concentrations were recorded for the 4-4 quadrants.

X-ray diffraction (XRD) analysis

Due to the shape of the samples, the XRD tests were carried out using Pb as a background (Pb gives reflections at known constant values of 2Θ). The diffractograms contained images of the tested samples and Pb. For the modified Ti surfaces, reflections from HA and Ti could be observed. The HA reflex at an angle of 25.8° 2Θ matching the (002) plane was recorded for almost all the samples (Fig. 3). The (113) plane matching the reflex at an angle of 35.4° 2Θ was overlapped by the reflexes from the Ti base, which may be attributed to a thin HA layer. Hydroxyapatite was not detected on quadrants A-4-4, C-4-4 and D-3-4. Based on the intensity of diffraction peaks for HA, we can order the quadrants as follows: C-2-4 > 1-4 > 3-4 > 4-4; B-1-4 > 4-4 > 3-4 > 2-4; D-1-4 > 4-4 > 2-4 > 3-4; A-1-4 > 2-4 > 3-4 >4-4, with the greatest concentration of HA on sample C.

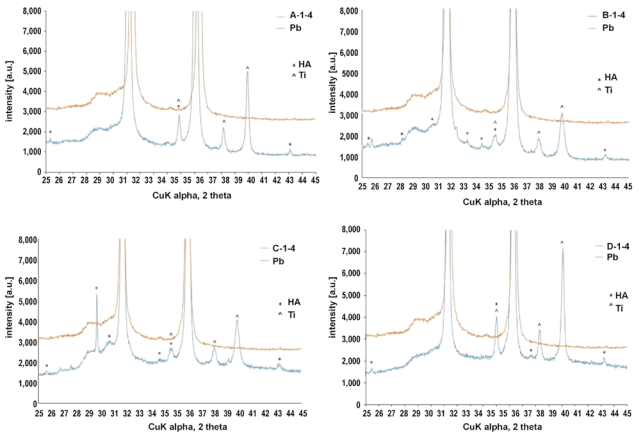

Fig. 3. X-ray diffraction (XRD) patterns in the angle range of the hydroxyapatite (HA) reflexes on one quadrant of each sample with the most intense HA peaks

Raman spectroscopy analysis

The Raman spectroscopy analysis confirmed the presence of HA on the 4th quadrant of all samples (Fig. 4). The presence of HA is manifested by the 4 bands appearing in the range 400–470 cm^{-1}, 550–650 cm^{-1}, 930–990 cm^{-1}, and 1,010–1,070 cm^{-1}, corresponding to the vibration in phosphate groups.[29,30] The single, most intensive and narrow band occurring at 960 cm^{-1} with a full width at half maximum equal to 15 cm^{-1} confirmed the presence of HA without substitution by other ions in the crystal lattice.[31] No other forms of calcium phosphates were detected. Raman spectroscopy did not identify HA on quadrants 1-4 to 3-4.

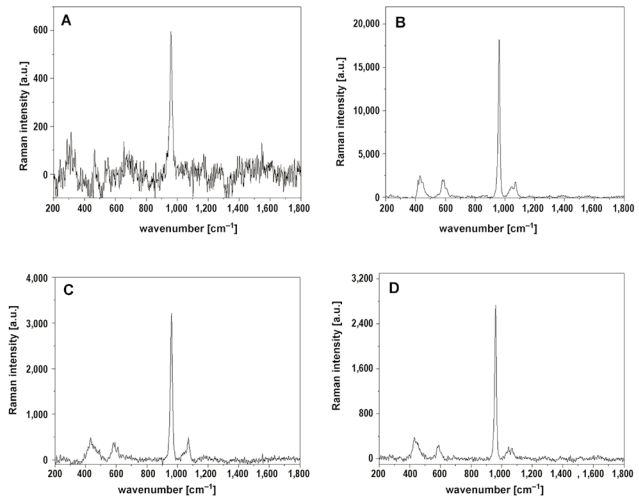

Fig. 4. Raman spectra of quadrants 4-4 for samples A–D

Contact angle studies

The contact angle analysis displayed a range of results from 20.51° up to 161.5° (Table 4). The most hydrophilic samples were B and C, with contact angles of 20.51° and 23.84°, respectively. These results were obtained for the 1-4 laser surface modification. The contact angles for samples A and D were greater than those of samples C and B. Laser modification 4-4 resulted in the highest contact angle for samples B and D.

Table 4. Contact angle of the hydroxyapatite (HA) coating after laser modification, quadrants 1-4 to 4-4

Sample and quadrant	Contact angle [°]
A-1-4	146.30 ±2.072
A-2-4	126.40 ±2.725
A-3-4	137.80 ±1.318
A-4-4	144.80 ±2.290
B-1-4	20.51 ±2.925
B-2-4	55.53 ±4.657
B-3-4	45.28 ± 3.110
B-4-4	56.27 ±5.523
C-1-4	23.84 ±6.031
C-2-4	53.30 ±4.362
C-3-4	85.84 ±0.952
C-4-4	36.89 ±5.965
D-1-4	153.20 ±0.426
D-2-4	145.30 ±2.133
D-3-4	136.40 ±0.289
D-4-4	161.50 ±1.033

Data presented as *M* ±*SD*.

Discussion

In the present study, 4 different techniques of HA laser modification on a Ti substrate were used. For the 1-4 laser modification, a combination of LIPSS and fusion was used, while for modifications 2-4 to 4-4, a sintering process with different parameters was implemented. The result of laser surface treatment depends on power density, which is correlated with the number of pulses and the speed of beam movement.

The 4-4 surface modification did not alter the crystal structure of the HA coating, as shown in the SEM images. The characteristics of the electrodeposited HA coating without laser modifications are discussed in our previous study.[17] On the other hand, modifications 1-4 up to 3-4 eliminated the crystal structure of HA, leaving spherical residues, as well as caused alterations in the Ti surface, leaving a microgroove pattern. In those surface modifications, the effects of laser melting and vaporization can be observed, since the crystal structures were transformed into spherical structures. Parallel grooves indicating LIPSS were also present on quadrants 2-4 and 3-4. The depth of the grooves which occurred after modifications 1-4 to 3-4 was the highest for the LIPSS and fusion modification and the lowest for the 3-4 modification procedure. The 1-4 up to 3-4 laser modifications resulted in the femtosecond laser ablation processing of Ti, leaving a microstructured surface. Such processing can influence the tribological properties of the surface and its wetting properties.[32] The microstructure of the parallel groves also had a positive effect on the osteoblast reaction by enhancing surface hydrophilicity, serum protein adsorption and osteoblast maturation.[33] Parallel grooves also facilitate cells expansion along the direction of the grooves, resulting in better coverage on the implant surface.[34]

An increase of the laser power by 0.2 W changed the morphology of HA, but did not cause its chemical degradation; HA peaks were found in the XRD spectra of quadrants 2-4 and 3-4 modified by laser with the highest power density. The crystal structure of the HA coating present on the 4-4 laser-conditioned quadrants proved to be osteoconductive, as shown in our previous study.[17]

Surface roughness, expressed as Ra, ranged from 1.32 μm to 1.85 μm. For most of the surfaces, laser modifications 1-4 and 2-4 resulted in the highest roughness values. However, for laser modifications 3-4 and 4-4, this parameter was lower. The Rt parameter, defined as the total height of the profile, was the greatest for the 1-4 and 2-4 laser modifications, with the C-2-4 sample exhibiting the greatest height of 17.12 μm. High Rt values were also noted for the D-4-4 sample, but this was correlated with the structure of the electrodeposited HA (i.e., the foci of long, needle-like crystals). The roughness of all the samples presented in this study can be defined as moderate.[34] As reported by Wennerberg and Albrektsson in a review of over 100 publications, implant surfaces of such roughness parameters can facilitate bone reaction better than smoother or even rougher surfaces.[34] Also, our previous studies proved positive osteoblast reactions for moderately rough Ti surfaces, expressed as increased osteoblast viability and differentiation.[35,36]

The analysis of the chemical composition of the samples revealed the presence of HA, although there were some differences between the EDS, XRD and Raman spectroscopy results. The XRD did not detect the presence of HA on quadrants A-4-4 and C-4-4, while Raman spectroscopy confirmed its presence on those quadrants. Such XRD results could be caused by instrumental limitations. The radiation might not have fallen on the sample due to its small size, or might only have fallen on it in a small percentage, since the distribution of Ca and P on the sample surface was not uniform. On the other hand, Raman spectroscopy detected the presence of HA only on quadrants 4-4, which, according to the EDS analysis, were the richest in Ca and P. The EDS revealed the presence of Ca and P in each quadrant of each sample, predominantly on quad-

rants 4-4. Raman spectroscopy also revealed that the HA present in the analyzed samples was pure, without substitution by other ions in the crystal lattice. Based on the analysis of the band occurring at 960 cm^{-1}, it can be stated that no other forms of calcium phosphates, such as tricalcium phosphate or tetracalcium phosphate, were present.

The weight percentages of Ca and P, based on the EDS analysis, for quadrants 4-4 comply with the thickness of the HA coating observed on the SEM images. The highest Ca and P concentrations were noted for sample B, then for D and C, and the lowest concentrations were observed for sample A. While analyzing the weight percentages of Ca and P on the sample surface, a pattern was found. The quadrants with the 4-4 laser modification presented the highest Ca and P concentrations, whereas the lowest were noted for the laser-sintered and fused quadrants. The same pattern can be observed in the O weight percentage. A similar pattern is observed in the results of the roughness analysis. The roughness Ra values are the lowest on the 4-4 quadrants and the highest on the laser-sintered and fused quadrants. The LIPSS and fusion, as well as the 2-4 and 3-4 modification processes, seem to increase the surface roughness while decreasing the Ca, P and O concentrations on the sample surface. The O weight percentage in the 4-4 quadrants is comparable with the result obtained for the samples before laser modification. The 2 remaining modification processes and the LIPSS and fusion process resulted in a decreased O concentration, with a higher reduction observed for the LIPSS and fusion quadrants. In the case of sample B – the sample with the richest HA coating – the 2-4 laser modification resulted in higher Ca and P concentrations than the 3-4 laser modification. This situation was opposite to the other samples.

Calcium phosphates have been reported to possess osteoinductive and osteoconductive characteristics.[37–43] Osteoinduction is the ability to induce progenitor cells to differentiate into osteoblastic lineages, while osteoconduction is the ability to promote bone growth on the surface of materials.[37] Such surface properties increase cell adhesion, differentiation and proliferation.[44] Cell adhesion is correlated with the ability to adsorb extracellular matrix (ECM) proteins, which, in turn, is related to such surface features as roughness, energy, crystallinity, and solubility.[37,44] An increased protein adsorption and cell adhesion are reported on calcium phosphate-coated implants.[37,45,46] Calcium phosphates also aid in the osteogenic differentiation of mesenchymal stem cells (MSCs).[37,47,48] The improved bone reaction of calcium phosphate-coated implants is also related to the entrapment of blood platelets on such surfaces and their activation. The activated platelets release biomolecules that can be retained by the fibrin matrix on the surface to facilitate the regeneration of the surrounding tissues.[40] Due to such surface features, calcium phosphate-coated implants are reported to present improved osseointegration.[17,38]

Quadrants 4-4 are the quadrants presenting the highest concentrations of Ca and P, with sample B exhibiting the highest concentrations of all of the samples. Based on the Ca and P concentrations, the B-4-4 quadrant should present the highest osteoinductive and osteoconductive properties, since calcium phosphates have been documented to possess biocompatible and osteoconductive properties.[16–18,36]

The presence of C on the analyzed sample surfaces can be associated with the presence of carbon dioxide (CO_2) and other organic molecules from the air.[49] Such carbon contamination, apart from roughness-induced hydrophobicity, is known to cause higher contact angles and lower surface energy, resulting in a surface with hydrophobic properties.[49–51] Rupp et al. reported a decreased water contact angle in samples after a 50% carbon reduction.[49] The reduction was from about 35 at% for the samples with a water contact angle of 122.40°–139.88° to the level of 15 at%, resulting in a water contact angle of 0°.[49] Hotchkiss et al. reported hydrophobic surface properties at a carbon concentration of ~43–44%.[51] In their study, a carbon level of ~30% resulted in a low contact angle and hydrophilic surface properties.[51] In the present study, the C concentration ranges from 0.48 wt% to 2.12 wt%, as revealed by the EDS analysis. The carbon levels are not reflected in the water contact angle results, which, according to the Rupp et al.'s study, should be at the level of 0°.[49] The C concentration in the present study is not correlated with the hydrophilicity of the surface. The highest C concentrations were reported for sample B, the richest in Ca and P. Lower carbon concentrations were noted for sample D, which also comes second according to the Ca and P concentrations. No correlation could be found between the C concentration and the type of laser conditioning.

Contact angle studies revealed a division of samples into 2 groups. A group of contact angles ranging from 20.51° to 85.84° consisted of samples B and C. Those samples can be classified as samples with hydrophilic surfaces. Samples A and D presented contact angles in the range of 126.4°–161.5° and could be classified as samples with hydrophobic surfaces. For the group of hydrophilic surfaces, the lowest result in both cases was noted for the 1-4 quadrants. Those quadrants also presented lower O concentrations, and are also the quadrants with the most intensive ablation. The correlation between the surface roughness and the surface wettability could not be established. While evaluating all 4 samples, the highest contact angle results were for quadrants 3-4 and 4-4.

The contact angle studies of the HA-coated, LIPSS plus fusion-modified quadrants of samples B and C revealed improved hydrophilic properties as compared to the LIPSS surfaces of uncoated Ti alloy studied by Schweitzer et al.[10] The contact angles of the LIPSS-modified surfaces reported by Schweitzer were similar to those of the HA-coated and sintered quadrants of the samples B and C.[10]

The enhanced surface hydrophilicity of the implant surface can result in the shortening of the osseointegration period, and increase the bond strength of the implant to bone tissue.[2] On the cellular level, hydrophilicity enhances protein adsorption, platelet aggregation, and monocyte and macrophage adhesion, increases the fibroblastic cell response, as well as the adhesion, differentiation and proliferation of osteoblasts.[37,52–54] Those events result in the acceleration of the healing process and bone formation in the initial period of osseointegration.[2,55–58] Hydrophilic surfaces can also increase the levels of alkaline phosphates, osteocalcin and bone sialoproteins, which are the differentiation markers of osteoblasts, indicating the osteoconductive potential of such surfaces.[2,54,59,60] The surface texture with parallel microgrooves was also reported to increase the surface hydrophilicity, along with serum protein adsorption and osteoblast maturation.[32,33] The phenomenon of increased hydrophilicity of micro-grooved Ti surfaces is related to altered surface chemistry.[32] A hydrophilic microrough Ti surface topography also elicits a macrophage phenotype associated with reduced inflammation and enhanced pro-osteogenic signaling.[61]

The laser modification of the HA coating resulted in 2 kinds of surfaces. Laser-induced periodic surface structure texturing could be observed on quadrants 1-4 to 3-4, with parallel grooves, and HA melted and sintered into spherical structures. The chemical composition of those quadrants had decreased Ca, P, O, and C concentrations. The 4-4 laser surface conditioning did not alter the needle-like morphology of the electrochemically deposited HA coating and caused only minor changes in the chemical composition of the surface. The contact angle studies revealed the presence of 2 groups: the hydrophilic group (B and C samples); and the hydrophobic group (A and D samples). The LIPSS–fusion modification decreased the water contact angle of the hydrophilic samples.

The surface with the most promising osteoconductive properties seems to be the B-1-4 sample with the optimal hydrophilic properties, LIPSS and the most intensive HA peaks based on the XRD analysis. Sample B-2-4 also presents favorable osteoconductive characteristics, such as high Ca and P concentrations, as shown by the EDS analysis, and LIPSS.

Further biological analyses are necessary to evaluate the cell and tissue response to such laser modifications of the HA coating on Ti. Also, testing the material toxicity, and the loading time and conditions would be beneficial for the analysis of the implant's dynamic integration with bone.[62–64]

Conclusions

The ultrashort-pulsed laser modification of the HA coating for regimes 1-4 to 3-4 resulted in the LIPSS texturing of the Ti surface with HA sinterization.

Further biological analyses are necessary to evaluate the cell and tissue response to such laser-modified HA coating on Ti.

Ethics approval and consent to participate

Not applicable.

Data availability

The datasets supporting the findings of the current study are openly available in Zenodo at https://doi.org/10.5281/zenodo.8398379.

Consent for publication

Not applicable.

Use of AI and AI-assisted technologies

Not applicable.

ORCID iDs

Magdalena Łukaszewska-Kuska https://orcid.org/0000-0002-4163-0995
Piotr Krawczyk https://orcid.org/0000-0001-6083-9316
Tomasz Buchwald https://orcid.org/0000-0003-1837-402X
Agnieszka Martyła https://orcid.org/0000-0001-5205-5052
Viktor Zinchenko https://orcid.org/0000-0002-5761-8616
Radomir Majchrowski https://orcid.org/0000-0002-4982-3265
Robert Edward Przekop https://orcid.org/0000-0002-7355-5803
Barbara Dorocka-Bobkowska https://orcid.org/0000-0003-3659-7761

References

1. Brånemark PI, Hansson BO, Adel R, et al. Osseointegrated implants in the treatment of the edentulous jaw. Experience from a 10-year period. *Scand J Plast Reconstr Surg*. 1977;16:1–132. PMID:356184.
2. Souza JC, Sordi MB, Kanazawa M, et al. Nano-scale modification of titanium implant surfaces to enhance osseointegration. *Acta Biomater*. 2019;94:112–131. doi:10.1016/j.actbio.2019.05.045
3. Lee JWY, Bance ML. Physiology of osseointegration. *Otolaryngol Clin North Am*. 2019;52(2):231–242. doi:10.1016/j.otc.2018.11.004
4. Günay-Bulutsuz A, Berrak Ö, Yeprem HA, Arisan ED, Yurci ME. Biological responses of ultrafine grained pure titanium and their sand blasted surfaces. *Mater Sci Eng C Mater Biol Appl*. 2018;91:382–388. doi:10.1016/j.msec.2018.05.056
5. Granato R, Bonfante EA, Castellano A, et al. Osteointegrative and microgeometric comparison between micro-blasted and alumina blasting/acid etching on grade II and V titanium alloys (Ti-6Al-4V). *J Mech Behav Biomed Mater*. 2019;97:288–295. doi:10.1016/j.jmbbm.2019.05.026
6. Bi Q, Song X, Chen Y, Zheng Y, Yin P, Lei T. Zn-HA/Bi-HA biphasic coatings on titanium: Fabrication, characterization, antibacterial and biological activity. *Colloids Surf B Biointerfaces*. 2020;189:110813. doi:10.1016/j.colsurfb.2020.110813
7. Lu M, Chen H, Yuan B, et al. Electrochemical deposition of nanostructured hydroxyapatite coating on titanium with enhanced early stage osteogenic activity and osseointegration. *Int J Nanomedicine*. 2020;15:6605–6618. doi:10.2147/IJN.S268372
8. Ogawa T. Ultraviolet photofunctionalization of titanium implants. *Int J Oral Maxillofac Implants*. 2014;29(1):e95–e102. doi:10.11607/jomi.te47
9. Schnell G, Jagow C, Springer A, Frank M, Seitz H. Time-dependent anisotropic wetting behavior of deterministic structures of different strut widths on Ti6Al4V. *Metals*. 2019;9(9):938. doi:10.3390/met9090938

10. Schweitzer L, Cunka A, Pereira T, et al. Preclinical in vitro assessment of submicron-scale laser surface texturing on Ti6Al4V. *Materials (Basel)*.2020;13(23):5342. doi:10.3390/ma13235342
11. Gaggl A, Schultes G, Müller WD, Kächer H. Scanning electron microscopical analysis of laser-treated titanium implant surfaces – a comparative study. *Biomaterials*. 2000;21(10):1067–1073. doi:10.1016/s0142-9612(00)00002-8
12. Schnell G, Duenow U, Seitz H. Effect of laser pulse overlap and scanning line overlap on femtosecond laser-structured Ti6Al4V surfaces. *Materials (Basel)*. 2020;13(4):969. doi:10.3390/ma13040969
13. Bonse J, Höhm S, Rosenfeld A, Krüger J. Sub-100-nm laser-induced periodic surface structures upon irradiation of titanium by Ti: Sapphire femtosecond laser pulses in air. *Appl Phys A*. 2013;110:547–551. doi:10.1007/s00339-012-7140-y
14. Uskoković V, Uskoković DP. Nanosized hydroxyapatite and other calcium phosphates: Chemistry of formation and application as drug and gene delivery agents. *J Biomed Mater Res B Appl Biomater*. 2011;96(1):152–191. doi:10.1002/jbm.b.31746
15. Koutsopoulos S. Synthesis and characterization of hydroxyapatite crystals: A review study on the analytical methods. *J Biomed Mater Res*. 2002;62(4):600–612. doi:10.1002/jbm.10280
16. Rajesh P, Muraleedharan CV, Komath M, Varma H. Laser surface modification of titanium substrate for pulsed laser deposition of highly adherent hydroxyapatite. *J Mater Sci Mater Med*. 2011;22(7):1671–1679. doi:10.1007/s10856-011-4342-3
17. Łukaszewska-Kuska M, Krawczyk P, Martyla A, Hędzelek W, Dorocka-Bobkowska B. Hydroxyapatite coating on titanium endosseous implants for improved osseointegration: Physical and chemical considerations. *Adv Clin Exp Med*. 2018;27(8):1055–1059. doi:10.17219/acem/69084
18. Le Guéhennec L, Soueidan A, Layrolle P, Amouriq Y. Surface treatments of titanium dental implants for rapid osseointegration. *Dent Mater*. 2007;23(7):844–854. doi:10.1016/j.dental.2006.06.025
19. Kim KH, Ramaswamy N. Electrochemical surface modification of titanium in dentistry. *Dent Mater J*. 2009;28(1):20–36. doi:10.4012/dmj.28.20
20. Ma M, Ye Wei, Wang XX. Effect of supersaturation on the morphology of hydroxyapatite crystals deposited by electrochemical deposition on titanium. *Mater Lett*. 2008;62(23):3875–3877. doi:10.1016/j.matlet.2008.05.009
21. Peng P, Kumar S, Voelcker NH, Szili E, Smart RStC, Griesser HJ. Thin calcium phosphate coatings on titanium by electrochemical deposition in modified simulated body fluid. *J Biomed Mat Res A*. 2006;76(2):347–355. doi:10.1002/jbm.a.30514
22. Kuo MC, Yen SK. The process of electrochemical deposited hydroxyapatite coatings on biomedical titanium at room temperature. *Mater Sci Eng C*. 2002;20(1–2):153–160. doi:10.1016/S0928-4931(02)00026-7
23. Maalouf M, Khali AA, Di Maio Y, et al. Polarization of femtosecond laser for titanium alloy nanopatterning influences osteoblastic differentiation. *Nanomaterials (Basel)*. 2022;12(10):1619. doi:10.3390/nano12101619
24. Cunha A, Zouani OF, Plawinski L, et al. Human mesenchymal stem cell behavior on femtosecond laser-textured Ti-6Al-4V surfaces. *Nanomedicine (Lond)*. 2015;10(5):725–739. doi:10.2217/nnm.15.19
25. Hu R, Lin CJ, Shi HY. A novel ordered nano hydroxyapatite coating electrochemically deposited on titanium substrate. *J Biomed Mater Res A*. 2007;80(3):687–692. doi:10.1002/jbm.a.30891
26. Ungureanu DN, Angelescu N, Ion RM, Stoian EV, Rizescu CZ. Synthesis and characterization of hydroxyapatite nanopowders by chemical precipitation. In: Bojkovic ZS, ed. *Recent Researches in Communications, Automation, Signal Processing, Nanotechnology, Astronomy and Nuclear Physics*. Conference proceedings. Cambridge, UK, February 20–22, 2011. WSEAS Press; 2011:296–301. https://www.researchgate.net/publication/262322346_Synthesis_and_characterization_of_hydroxyapatite_nanopowders_by_chemical_precipitation#full-text.
27. Lee SW, Hahn BD, Kang TY, et al. Hydroxyapatite and collagen combination-coated dental implants display better bone formation in the peri-implant area than the same combination plus bone morphogenetic protein-2-coated implants, hydroxyapatite only coated implants, and uncoated implants. *J Oral Maxillofac Surg*. 2014;72(1):53–60. doi:10.1016/j.joms.2013.08.031
28. Angelescu N, Ungureanu DN, Anghelina FV. Synthesis and characterization of hydroxyapatite obtained in different experimental conditions. *Sci Bull Valahia Univ Mater Mech*. 2011;9(6):15–18. https://www.researchgate.net/publication/281206966_Synthesis_and_characterization_of_hydroxyapatite_obtained_in_different_experimental_conditions#full-text
29. Buchwald T, Buchwald Z. Assessment of the Raman spectroscopy effectiveness in determining the early changes in human enamel caused by artificial caries. *Analyst*. 2019;144(4):1409–1419. doi:10.1039/c8an01494a
30. Buchwald T, Okulus Z, Szybowicz M. Raman spectroscopy as a tool of early dental caries detection – new insights. *J Raman Spectrosc*. 2017;48(8):1094–1102. doi:10.1002/jrs.5175
31. Okulus Z, Sandomierski M, Zielińska M, Buchwald T, Voelkel A. Zeolite fillers for resin-based composites with remineralizing potential. *Spectrochim Acta A Mol Biomol Spectrosc*. 2019;210:126–135. doi:10.1016/j.saa.2018.11.020
32. Raimbault O, Benayoun S, Anselme K, et al. The effects of femtosecond laser-textured Ti-6Al-4V on wettability and cell response. *Mater Sci Eng C Mater Biol Appl*. 2016;69:311–320. doi:10.1016/j.msec.2016.06.072
33. Lee SW, Lee MH, Oh N, Park JA, Leesungbok R, Ahn AJ. Correlation between surface hydrophilicity and osteoblastic differentiation on microgrooved titanium substrata. *J Oral Implantol*. 2012;38(1):11–19. doi:10.1563/AAID-JOI-D-09-00144.1
34. Wennerberg A, Albrektsson T. Effects of titanium surface topography on bone integration: A systematic review. *Clin Oral Implants Res*. 2009;20(Suppl 4):172–184. doi:10.1111/j.1600-0501.2009.01775.x
35. Lukaszewska-Kuska M, Wirstlein P, Majchrowski R, Dorocka-Bobkowska B. Osteoblastic cell behaviour on modified titanium surfaces. *Micron*. 2018;105:55–63. doi:10.1016/j.micron.2017.11.010
36. Lukaszewska-Kuska M, Wirstlein P, Majchrowski R, Dorocka-Bobkowska B. The effects of titanium topography and chemical composition on human osteoblast cell. *Physiol Res*. 2021;70(3):413–423. doi:10.33549/physiolres.934582
37. Jeong J, Kim JH, Shim JH, Hwang NS, Heo CY. Bioactive calcium phosphate materials and applications in bone regeneration. *Biomater Res*. 2019;23:4. doi:10.1186/s40824-018-0149-3
38. Nikolidakis D, van den Dolder, Wolke JG, Jansen JA. Effect of platelet-rich plasma on the early bone formation around Ca-P-coated and non-coated oral implants in cortical bone. *Clin Oral Implants Res*. 2008;19(2):207–213. doi:10.1111/j.1600-0501.2007.01456.x
39. Hayakawa T, Yoshinari M, Nemoto K, Wolke JG, Jansen JA. Effect of surface roughness and calcium phosphate coating on the implant/bone response. *Clin Oral Implants Res*. 2000;11(4):296–304. doi:10.1034/j.1600-0501.2000.011004296.x
40. Nakamura M, Aizawa H, Kawabata H, et al. Platelet adhesion on commercially pure titanium plates in vitro III: Effects of calcium phosphate-blasting on titanium plate biocompatibility. *Int J Implant Dent*. 2020;6(1):74. doi:10.1186/s40729-020-00270-2
41. Civantos A, Martínez-Campos E, Ramos V, Elvira C, Gallardo A, Abarrategi A. Titanium coatings and surface modifications: Toward clinically useful bioactive implants. *ACS Biomater Sci Eng*. 2017;3(7):1245–1261. doi:10.1021/acsbiomaterials.6b00604
42. de Groot K, Wolke JG, Jansen JA. Calcium phosphate coatings for medical implants. *Proc Inst Mech Eng H*. 1998;212(2):137–147. doi:10.1243/0954411981533917
43. Junker R, Dimakis A, Thoneick M, Jansen JA. Effects of implant surface coatings and composition on bone integration: A systematic review. *Clin Oral Implants Res*. 2009;20(Suppl 4):185–206. doi:10.1111/j.1600-0501.2009.01777.x
44. Samavedi S, Whittington AR, Goldstein AS. Calcium phosphate ceramics in bone tissue engineering: A review of properties and their influence on cell behavior. *Acta Biomater*. 2013;9(9):8037–8045. doi:10.1016/j.actbio.2013.06.014
45. Surmenev RA, Surmaneva MA, Ivanova AA. Significance of calcium phosphate coatings for the enhancement of new bone osteogenesis – a review. *Acta Biomater*. 2014;10(2):557–579. doi:10.1016/j.actbio.2013.10.036
46. Fujii E, Ohkubo M, Tsura K, et al. Selective protein adsorption property and characterization of nano-crystalline zinc-containing hydroxyapatite. *Acta Biomater*. 2006;2(1):69–74. doi:10.1016/j.actbio.2005.09.002

47. Orimo H. The mechanism of mineralization and the role of alkaline phosphatase in health and disease. *J Nippon Med Sch*. 2010;77(1):4–12. doi:10.1272/jnms.77.4
48. Komori T. Regulation of osteoblast differentiation by Runx2. *Adv Exp Med Biol*. 2010:658:43–49. doi:10.1007/978-1-4419-1050-9_5
49. Rupp F, Scheideler L, Olshanska N, de Wild M, Wieland M, Geis-Gerstorfer J. Enhancing surface free energy and hydrophilicity through chemical modification of microstructured titanium implant surfaces. *J Biomed Mater Res A*. 2006;76(2):323–334. doi:10.1002/jbm.a.30518
50. Massaro C, Rotolo P, De Riccardis F, et al. Comparative investigation of the surface properties of commercial titanium dental implants. Part I: Chemical composition. *J Mater Sci Mater Med*. 2002;13(6):535–548. doi:10.1023/a:1015170625506
51. Hotchkiss KM, Ayad NB, Hyzy SL, Boyan BD, Olivares-Navarrete R. Dental implant surface chemistry and energy alter macrophage activation in vitro. *Clin Oral Implants Res*. 2017;28(4):414–423. doi:10.1111/clr.12814
52. Mendonça G, Mendonça DB, Aragão FJ, Cooper LF. Advancing dental implant surface technology – from micron- to nanotopography. *Biomaterials*. 2008;29(28):3822–3835. doi:10.1016/j.biomaterials.2008.05.012
53. Zhao G, Raines AL, Wieland M, Schwartz Z, Boyan BD. Requirement for both micron- and submicron scale structure for synergistic responses of osteoblasts to substrate surface energy and topography. *Biomaterials*. 2007;28(18):2821–2829. doi:10.1016/j.biomaterials.2007.02.024
54. Nagasawa M, Cooper LF, Ogino Y, et al. Topography influences adherent cell regulation of osteoclastogenesis. *J Dent Res*. 2016;95(3):319–326. doi:10.1177/0022034515616760
55. Chambrone L, Shibli JA, Mercúrio CE, Cardoso B, Preshaw PM. Efficacy of standard (SLA) and modified sandblasted and acid-etched (SLActive) dental implants in promoting immediate and/or early occlusal loading protocols: A systematic review of prospective studies. *Clin Oral Implants Res*. 2015;26(4):359–370. doi:10.1111/clr.12347
56. Kopf BS, Schipanski A, Rottmar M, Berne S, Maniura-Weber K. Enhanced differentiation of human osteoblasts on Ti surfaces pre-treated with human whole blood. *Acta Biomater*. 2015;19:180–190. doi:10.1016/j.actbio.2015.03.022
57. Wennerberg A, Jimbo R, Stübinger S, Obrecht M, Dard M, Berner S. Nanostructures and hydrophilicity influence osseointegration: A biomechanical study in the rabbit tibia. *Clin Oral Implants Res*. 2014;25(9):1041–1050. doi:10.1111/clr.12213
58. Philipp A, Duncan W, Roos M, Hämmerle CH, Attin T, Schmidlin PR. Comparison of SLA® or SLActive® implants placed in the maxillary sinus with or without synthetic bone graft materials – an animal study in sheep. *Clin Oral Implants Res*. 2014;25(10):1142–1148. doi:10.1111/clr.12255
59. Hyzy SL, Olivares-Navarrete R, Ortman S, Boyan BD, Schwartz Z. Bone morphogenetic protein 2 alters osteogenesis and anti-inflammatory profiles of mesenchymal stem cells induced by microtextured titanium in vitro. *Tissue Eng Part A*. 2017;23(19–20):1132–1141. doi:10.1089/ten.TEA.2017.0003
60. Lang NP, Salvi GE, Huynh-Ba G, Ivanovski S, Donos N, Boosshardt DD. Early osseointegration to hydrophilic and hydrophobic implant surfaces in humans. *Clin Oral Implants Res*. 2011;22(4):349–356. doi:10.1111/j.1600-0501.2011.02172.x
61. Hamlet SM, Lee RS, Moon HJ, Alfarsi MA, Ivanovski S. Hydrophilic titanium surface-induced macrophage modulation promotes pro-osteogenic signalling. *Clin Oral Implants Res*. 2019;30(11):1085–1096. doi:10.1111/clr.13522
62. Shamel M, Rady D, Al Ankily M. Evaluation of lingual mucosa toxicity and recovery follow-up in rats, following sub-chronic exposure to titanium dioxide nanoparticles. *Dent Med Probl*. 2022;59(3):427–435. doi:10.17219/dmp/137904
63. Krawiec M, Olchowy C, Kubasiewicz-Ross P, Hadzik J, Dominiak M. Role of implant loading time in the prevention of marginal bone loss after implant-supported restorations: A targeted review. *Dent Med Probl*. 2022;59(3):475–481. doi:10.17219/dmp/150111
64. Reda R, Zanza A, Galli M, De Biase A, Testarelli L, Di Nardo D. Applications and clinical behavior of BioHPP in prosthetic dentistry: A short review. *J Compos Sci*. 2022;6(3):90. doi:10.3390/jcs6030090